Journal of Materials Chemistry A

Accepted Manuscript

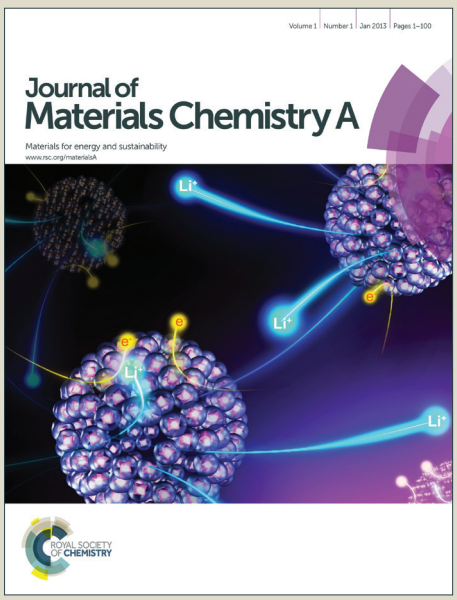

ROYAL SOCIETY OF CHEMISTRY

www.rsc.org/materialsA

Super Biosorbent from Dendrimer Poly(amidoamine)-Grafted Cellulose Nanofibril Aerogels for Effective Removal of Cr(VI)

Jiangqi Zhao, Xiaofang Zhang, Xu He, Meijie Xiao, Wei Zhang* and Canhui Lu*

State Key Laboratory of Polymer Materials Engineering, Polymer Research Institute at Sichuan University, Chengdu 610065, China.

** Authors for correspondence: E-mail: weizhang@scu.edu.cn (W. Zhang), canhuilu@263.net (C. Lu); Phone: 86-28-85460607; Fax: 86-28-85402465.*

Abstract

During the past decades, heavy metal ions, especially hexavalent chromium [Cr(VI)], have substantially ravaged aquatic environment and human health. Thus, the development of new, more efficient, and environmentally friendly methods to tackle this problem becomes very urgent. In this study, a novel dendrimer poly(amidoamine)-grafted cellulose nanofibrils (PAMAM-g-CNFs) aerogel was synthesized for Cr(VI) removal. The morphology, structure and adsorption properties of the PAMAM-g-CNFs aerogel were investigated in detail. The results indicated the aerogel bore abundant functional groups with a bimodal pore structure and a high specific surface area, all of which are essential for an efficient adsorbent. The maximum Cr(VI) removal capacity of the aerogel reached 377.36 mg/g, the highest one ever reported for biosorbents. It was interesting to notice that part of Cr(VI) ions had been reduced to Cr(III) during the adsorption process, which meant PAMAM-g-CNFs could detoxify Cr(VI).

Introduction

Contamination by heavy metal ions gives rise to detrimental effects on the environment and human health. Among these hazardous heavy metal species, chromium (Cr) is one of priority pollutants in water resulting from numerous industrial activities.[1] Of the two most common oxidation states, Cr(VI) is known to be

highly toxic, mutagenic and carcinogenic to living organisms, whereas Cr(III) serves as a nontoxic substance and is an essential trace metal in human nutrition.[2] Various strategies have been proposed for Cr(VI) removal from waste water, including precipitation, ion exchange, membrane separation, and adsorption.[3,4] Adsorption is one of the most commonly used methods, due to its simplicity, effectiveness, ease of operation and reusability.[4]

Being abundant, cheap and environmentally benign, biosorbents have received increasing attention for the removal of heavy metals in recent years.[5] Many biomaterials such as pinus brutia,[6] wheat bran,[7] wool,[8] cellulose,[9] and so on, have been utilized for Cr(VI) removal. Cellulose is the most abundant natural polymer available worldwide.[10] Owing to its renewable, biodegradable and inexhaustible attributes, cellulose has been expected to become a key source of sustainable materials on an industrial scale.[11] However, compared with conventional adsorbents, the adsorption properties of biosorbents are not satisfactory.

The performance of adsorbents depends mainly on the specific surface area of the materials and the amount of functional groups responsible for adsorption.[12,13] In the past decade, nanocellulose has attracted great research interests.[11] Nanocellulose, in particular cellulose nanofibrils (CNFs), exhibits many other unique characteristics, such as large specific surface area, high aspect ratio, ease of chemical modification, and the ability to form highly porous mesh,[10,14,15] which make it great potential as the precursor to produce effective adsorbent materials. Dendrimers are highly branched macromolecules with a three-dimensional (3D) tree-like architecture. They can have well-defined molecular weights, sizes, and plenty of surface functionalities, demonstrating versatile characteristics desired for a broad range of applications, including supramolecular chemistry, sensing, catalysts, biomedical engineering and pollution control.[16] Poly(amidoamine) (PAMAM) is one of the most commonly investigated dendrimers.[17,18] It has a large number of amine groups and amide groups, as well as numerous cavities.[16] Those functional groups together with the unique molecular structure provide ideal building blocks to fabricate supersorbents for the removal of toxic anions, such as Cr(VI), in acidic conditions.[19]

In this study, CNFs were extracted from bamboo pulp through ultrasonication coupled with high shear homogenization. PAMAM-g-CNFs was synthesized by repeating the Michael reaction of methyl acrylate (MA) to amine groups on the modified CNFs (G0), followed by amidation of terminal ester groups with ethylenediamine (EDA).[16] Finally, the obtained PAMAM-g-CNFs was transformed into aerogels, which constitute an important class of porous materials with low density, high specific surface area and great adsorption properties.[15,20] The morphology, structure and adsorption properties of the materials were analyzed and discussed.

Experimental

Materials

Never-dried moso bamboo pulp was supplied by Yongfeng Paper Co., Ltd. (Sichuan, China). Its cellulose content was higher than 93% as reported by the supplier. Methyl acrylate (MA), ethylenediamine (EDA) and other chemicals were of analytical grade and supplied by Chengdu Kelong Chemicals Co., Ltd. (Sichuan, China).

Preparation of CNFs

The bamboo pulp was dispersed in distilled water at a solid concentration of 0.5 wt%. A horn-type ultrasonic generator (JY993IIDN, Scientz, China) was used to treat the suspension at an output power of 1,200 W for 30 min. Then, a high shear homogenizer (T18, IKA, Germany) was used to isolate CNFs at a rotation speed of 20,000 rpm for 1 h.

Preparation of PAMAM-g-CNFs

First, amine groups were introduced onto the surface of CNFs. 1 g CNFs was dispersed in 100 mL distilled water under nitrogen atmosphere and 1.5 g methyl methacrylate was slowly added with cerium ammonium nitrate (6 mM) as an initiator. This free radical reaction was conducted at room temperature for 3 h under magnetic stirring. The products were incubated with 1.5 g EDA in a methanol solution. The transesterification reaction lasted for 24 h at 60 ^{o}C under magnetic stirring. The

as-prepared amine-modified CNFs was purified through repeated methanol washing and marked as G0. Then the grafting of dendrimer PAMAM onto the CNFs was implemented by repeating two reactions: (1) Michael addition of MA to amine groups on the surface, and (2) amidation of terminal ester groups with EDA. Michael addition was performed as follows: 1 g G0 was dispersed in 100 mL methanol, followed by the addition of 1.5 g of MA. The mixture was stirred at 50 ^{o}C for 24 h. The product was washed with methanol repeatedly and labeled as G0.5. The amidation of terminal ester groups was carried out as follows: 1 g G0.5 and 1.5 g EDA were mixed in 100 mL methanol for amidation reaction which lasted for 24 h at 60 ^{o}C under magnetic stirring. The two reactions were repeated and the products were marked as G1, G3, G5 according to the repetition numbers.

Preparation of PAMAM-g-CNFs aerogel

The obtained PAMAM-g-CNFs was re-dispersed in distilled water at a solid concentration of about 1 wt%. The suspension was rapidly frozen in liquid nitrogen (-196 ^{o}C) and placed in a freeze-drying chamber (FD31A350, Biocool, China). The freeze-drying process was maintained at -30 ^{o}C for 72 h to produce well-shaped 3D aerogels.

Material characterization

The morphologies of cellulose fibers, PAMAM-g-CNFs, and cross-sectional regions of aerogel were observed using Inspect F50 scanning electron microscopy. The specific surface area of the aerogel was determined by nitrogen adsorption using Quantachrome NovaWin instrument and Brunauer-Emmett-Teller (BET) method. The chemical structure of samples was characterized by FTIR and XPS, respectively. FTIR analysis was performed from 4000 to 500 cm^{-1} at a resolution of 2 cm^{-1} using a Nicolet 560 FTIR spectrometer. XPS spectra were recorded on a Kratos XASAM 800 spectrometer with an Al Kα X-ray source (1486.6 eV). Zeta potential of the materials was measured using Zetasizer Nano ZS90 (Malvern Instruments Co., Britain). The materials were suspended in 0.1 mM NaCl solution. HCl and NaOH solutions were employed to adjust the pH values. The measurement was repeated for 3 times and the average value was adopted.

Adsorption experiments

A series of batch adsorption experiments were conducted for investigation of the effect of pH, contacting time, temperature, coexisting ions on the Cr(VI) removal capacity. The pH dependent adsorption behaviors were studied in the pH range from 1 to 10 adjusted by 0.1 mol/L HCl or NaOH solutions. The effect of initial Cr(VI) concentration (from 10 to 600 mg/L) on the adsorption performance was studied at pH=2 for 10 h. Meanwhile, the effect of contacting time was examined up to 24 h at pH=2. After adsorption, the Cr-loaded PAMAM-g-CNFs was regenerated using 0.1 mol/L NaOH and washed several times with distilled water to eliminate residue Cr(VI) traces. Then the regenerated PAMAM-g-CNFs was re-freeze-dried into aerogel and used again for Cr(VI) removal. The analyses of Cr(VI) in aqueous samples were performed using a UV-vis spectrophotometer at 540 nm after complexation with 1,5-diphenylcarbazide.[21] Total concentrations of chromium in the samples were measured by an atomic absorption spectroscopy (AA800, Perkin–Elmer, USA), and the concentration of Cr(III) was then calculated from the difference between the total Cr and Cr(VI) concentrations.

Results and discussion

Characterization of materials

Figure 1a and b showed 0.1 wt% dispersions of original cellulose fibers (OCFs) and CNFs after being left to stand for 3 days. Clear sedimentation was observed for the OCFs, whereas the CNFs were homogeneously dispersed in water without noticeable sedimentation. Regular cellulose fibers had an average diameter of 10 μm (Figure S1a). By contrast, after the mechanical extraction, the cellulose fibers were almost completely disintegrated into CNFs with diameters in the range of 20-50 nm (Figure S1b). The modified CNFs (Figure S1c) exhibited obviously thicker fiber diameters (50-150 nm) as compared with the precursor CNFs, which was consistent with the successful grafting of PAMAM. The resultant PAMAM-g-CNFs aerogel, with pale orange color, had an extremely low density (0.01 g/cm^3) and a high porosity

(99.39 %). Remarkably, the ultralight weight PAMAM-g-CNFs aerogel could stand stably on top of a lily stamen (Figure 2a). The PAMAM-g-CNFs aerogel had an open-cell geometry with pore sizes in the range of 5-30 μm, and these cells were almost interconnected through sheet-like "walls" (Figure 2b). Interestingly, zooming in on a single "wall" (the inset image in Figure 2b) revealed that the "wall" consisted of numerous minor pores with sizes of 50-200 nm. Such a bimodal pore structure had special significance for the adsorption, where the major pores were conducive to mass diffusion, and the minor pores were beneficial to improve the surface area. The specific surface area of the PAMAM-g-CNFs aerogel was determined to be 82 m^2/g by Brunauer−Emmett−Teller (BET) analysis, much higher than that of OCFs aerogel (0.8 m^2/g), representing a great advantage for adsorption.

The chemical structure of the PAMAM-g-CNFs was analyzed by Fourier transform infrared spectroscopy (FTIR). Compared with unmodified CNFs, an absorption peak at 1740 cm^{-1} appeared in the spectra of PAMAM-g-CNFs due to the presence of ester groups (Figure 2c). It revealed that methyl methacrylate had been grafted to CNFs, and the reaction between esters and ethylenediamine was incomplete for this solid–liquid reaction.[22] The intensity of absorbance at 1740 cm^{-1} significantly decreased after repeating the dendrimer modification. The absorption peaks at 1650, 1560 and 1450 cm^{-1} were assigned to amide and amine groups.[22,23] The relative intensities of these peaks were found to increase with increased reaction cycles. In addition, X-ray photoelectron spectroscopy (XPS) was used to characterize the PAMAM-g-CNFs in a quantitative manner. The XPS spectra of these samples were shown in Figure 2d and Figure S2. Compared with unmodified CNFs, new peaks appeared at around 399.3 eV for PAMAM-g-CNFs, which corresponded to nitrogen atom.[24] It was convinced that no nitrogen was detected in CNFs, while the nitrogen content in PAMAM-g-CNFs increased significantly with dendrimer generation increasing, and it reached 8.95% for G5. This suggested that PAMAM had been successfully grafted onto CNFs by repeating the reaction with EDA and MA. Consequently, a wealth of nitrogen-containing groups was introduced to the surface of aerogel, providing abundant adsorption sites for Cr(VI) removal.

Zeta potential characterizes essential surface properties of materials, especially the electric charge.[25] The zeta potentials of pristine and modified CNFs in solutions at different pH were illustrated in Figure S3. The pristine CNFs had an isoelectric point (i.e.p.) at around pH 2.2. In contrast, the i.e.p. of PAMAM-g-CNFs increased gradually with increased reaction cycles, and it shifted to a much higher value of 9.6 for G5 due to the enhanced protonation of amine groups on the dendrimer.[26] As a result, the zeta potential of G5 was positive at pH < 9.6, while for pristine CNFs the pH should be lower than 2.2. PAMAM-g-CNFs aerogels became more positively charged than pristine CNFs under acidic conditions. From the electrostatic interaction point of view, the PAMAM-g-CNFs could provide better adsorption performance for anionic adsorbates than the pristine CNFs, since the surface interactions between the adsorbent and the adsorbate were enhanced.[26]

Influence of solution pH

The pH value is one of the most important factors that can affect the adsorption behavior remarkably because it determines the charge density of the adsorbent and the present state of the analytes in solution.[27] The effect of pH on Cr(VI) removal over the range of 1-10 was investigated (Figure 3a). As expected, the G5 showed distinctly higher Cr(VI) removal capacity than CNFs throughout the pH range. For G5, the highest Cr(VI) removal was observed at pH 2. In this condition, the removal capacity of PAMAM-g-CNFs was as high as 335.16 mg/g, more than 10 times that of CNFs. The effect of solution pH could be tentatively explained by considering the surface charge of the adsorbent and the ionic forms of adsorbate. Under acidic conditions, amine groups could be protonated to form positively charged sites, e.g. $-NH_3^+$ groups, and electrostatic attraction occurred between Cr(VI) ions and $-NH_3^+$.[27] When pH increased, the concentration of H^+ in solution decreased. It became difficult for $-NH_2$ to be protonated, and at the same time the concentration of OH^- increased, which competed with Cr(VI) ions. Hence, the Cr(VI) removal capability declined at a higher pH. In addition, Cr (VI) exists in various forms such as H_2CrO_4, $HCrO_4^-$, CrO_4^{2-}, $HCr_2O_7^-$, and $Cr_2O_7^{2-}$ as a function of pH and concentration. The existing balances among different ionic species of chromium are shown as follows:[28]

$H_2CrO_4 \rightleftharpoons H^+ + HCrO_4^-$ (1)

$HCrO_4^- \rightleftharpoons H^+ + CrO_4^{2-}$ (2)

$2HCrO_4^- \rightleftharpoons Cr_2O_7^{2-} + H_2O$ (3)

At a lower pH (nearly 2), the Cr (VI) species are mostly in their univalent forms ($HCrO_4^-$) which require only one exchange site and are more likely to be adsorbed. However, when pH further decreases (lower than 2), H_2CrO_4 becomes the dominant species,[28] which can not be electrostatically attracted by the $-NH_3^+$ groups, leading to the decrease of removal capability.

It is noteworthy that the effluent from chromium industries is usually acidic, even strongly acidic in some cases, for example, the chromium-plating waste water.[29,30] Therefore, the aerogel biosorbent with its maximum Cr(VI) adsorption at a low pH is of great advantages for Cr(VI) removal, in particular in treating chromium-plating waste water.

Adsorption isotherms study

To examine the relationship between adsorbent and adsorbate at equilibrium and to estimate the maximum adsorption capacity of adsorbent, the effect of Cr(VI) concentration on adsorption was analyzed and the data were fitted with the Langmuir model (eq 4)[31] and the Freundlich model (eq 5),[32] respectively:

$$q_e = \frac{q_m K_L C_e}{1 + K_L C_e} \quad (4)$$

$$q_e = K_F C_e^{\frac{1}{n}} \quad (5)$$

where C_e (mg/L) is the equilibrium concentration of Cr(VI) in solution, q_e is the equilibrium adsorption capacity, q_m is the maximum adsorption capacity, K_L and K_F are constants for Langmuir and Freundlich isotherms, respectively, n is a Freundlich constant relating to adsorption intensity of the adsorbents.

The adsorption isotherms and fitting results were shown in Figure 3b and Table S1. Compared with Freundlich isotherm, the Langmuir isotherm could better describe the adsorption behaviors with a higher correlation coefficient ($R^2 = 0.9951$), indicating the

monolayer adsorption of Cr(VI) onto the PAMAM-g-CNFs surface.[31] The maximum adsorption capacity of G5 was calculated to be 377.36 mg/g, much higher than those for many other biosorbents (Table 1). To the best of our knowledge, this is the highest Cr(VI) adsorption capacity for any biosorbents reported so far. Furthermore, the effect of nitrogen content on adsorption capacity of Cr(VI) was studied and the results were illustrated in Figure 3c. The nitrogen content increased with the increase of dendrimer generation. As a result, the corresponding adsorption property was enhanced consistently.

To demonstrate the excellent adsorption performance of PAMAM-g-CNFs in a more intuitive manner, the Cr(VI) solution before and after adsorption was pictured and shown in Figure 3. The Cr(VI) aqueous solution (200 mg/g) was chartreuse in color (Figure 3d), and it turned into wine red after complexation with 1,5-diphenylcarbazide (Figure 3f). Also, the printed number on the backside of the bottle could not be seen. After adsorption, the pure Cr(VI) solution became colorless (Figure 3e), while the Cr(VI) complexation solution turned into light pink with high transparency. The backside number on the bottle was clearly visible.

The outstanding adsorption properties of PAMAM-g-CNFs aerogel were highly dependent on its well designed structures at both molecular and microscopic levels, which were summarized as follows: (1) The nitrogen content in the PAMAM-g-CNFs was as high as 8.95%. After PAMAM grafting, many amine groups had been tethered on the CNFs' surface, which could be protonated to attract Cr(VI) ions electrostatically under acidic conditions. (2) The PAMAM molecule had a 3D tree-like architecture with high hydrophilicity. Those functional groups could be fully exposed to interact with ions in aqueous solutions.[19] Moreover, PAMAM dendrimers generated numerous cavities in the interior. Those pocket-like cavities were very favorable for ions adsorption and storage.[18] (3) The precursor CNFs had nanometer dimensions, which provided a foundation for the final materials with large specific surface area. This is of particular importance for the biosorbents, since adsorption mainly happens at materials' surface.[12] (4) Finally, the obtained PAMAM-g-CNFs aerogel exhibited a high porosity coupled with a unique bimodal pore structure,

leading to fast adsorption rate and high adsorption capacity.

Adsorption kinetics and thermodynamics study

The study of adsorption kinetics is significant as it provides valuable insights into the adsorption rate and the mechanism of the adsorption.[40] The experimental data were analyzed using the pseudo-second-order equation (eq 6) as follows.[40]

$$\frac{t}{q_t} = \frac{1}{k_2 q_e^2} + \left(\frac{1}{q_e}\right) t \tag{6}$$

where q_e is the adsorption capacity (mg/g) at equilibrium, q_t is the adsorption capacity at time t, k_2 (g/mg·h) is the rate constant of pseudo-second-order adsorption.

As shown in Figure 4a, the adsorption rate of Cr(VI) on PAMAM-g-CNFs was initially quite high and then gradually reached equilibrium in 2 h. The linear fitting of experimental data and correlation kinetics parameters were shown in the insert of Figure 4a and Table S2, respectively. The plot appeared in good linearity with a high correlation coefficient (R^2 = 0.9996), and the theoretical q_e value (338.98 mg/g) was very close to the experimental data (335.99 mg/g), suggesting that these kinetics data were fitted very well by the pseudo-second-order equation and the removal of Cr(VI) was a chemisorption process.[40]

Thermodynamic parameters such as Gibbs free energy (ΔG^o), enthalpy (ΔH^o) and entropy (ΔS^o) were calculated using the following equations:[41]

$$K_c = \frac{C_{Ae}}{C_e} \tag{7}$$

$$\Delta G^o = -RT \ln K_c \tag{8}$$

$$\log K_c = \frac{\Delta S^o}{2.303R} - \frac{\Delta H^o}{2.303RT} \tag{9}$$

where K_c is the equilibrium constant, C_e is the equilibrium concentration in solution (mg/L) and C_{Ae} is the solid phase concentration at equilibrium (mg/L).

The effect of temperature on Cr(VI) removal was investigated and the results were shown in Figure 4b and Table S3. An increase in Cr(VI) removal with increasing

temperature together with the positive ΔH^o indicated that the Cr(VI) adsorption was an endothermic process. This was in accordance with the fact that Cr(VI) ions were partially reduced to Cr(III) during the adsorption, which had been proved to be an endothermic process.[21] The negative values of ΔG^o at various temperatures indicated the spontaneous nature of the adsorption process.[41] These results indicated that it was more favorable for Cr(VI) removal at higher temperatures.

Adsorption mechanism

To explore the possible mechanism of Cr(VI) adsorption by the dendrimer PAMAM modified CNFs aerogel, additional experiments were performed. XPS was used to investigate the surface chemical composition of the Cr(VI)-adsorbed PAMAM-g-CNFs (Figure S4 and 4a). There was a new Cr absorption peak on the aerogel (Figure S4). Interestingly, the high resolution XPS spectrum of the Cr 2p region (Fig. 4a) suggested that the Cr $2p_{1/2}$ and Cr $2p_{3/2}$ line peaks were located at 586.7 and 578.3 to 576.6 eV. However, the two peaks of Cr 2p3/2 at 578.3 and 576.6 eV were assigned to Cr(VI) and Cr(III), respectively.[27,42] It indicated that both Cr(VI) and Cr(III) coexisted on the surface of aerogel, and part of Cr(VI) had been reduced to Cr(III) during the adsorption process. The spectra of Cr 2p implied that the Cr bound to the aerogel was mainly in the trivalent form. The remaining negatively charged groups on CNFs, e.g., carboxyl groups, should be responsible for Cr(III) binding on the aerogel.[43] Besides, the valence and concentration of Cr in the solution were investigated by UV-Vis spectrophotometer and atomic absorption spectroscopy, and the results were shown in Figure 4b. The concentration of Cr(VI) decreased rapidly in the first 20 min (79.70%), which was attributed to the electrostatic attraction between Cr(VI) ions and the protonated amine groups on PAMAM-g-CNFs. On the other hand, Cr(III) ions, which were absent in the initial solution, appeared in the aqueous phase and their concentration increased continuously with time. The coexistence of Cr(VI) and Cr(III) in both biosorbent and aqueous phase indicated the removal of Cr(VI) was accompanied by a redox reaction. Some of the Cr(VI) ions were reduced to Cr(III) during the adsorption process. It has been well recognized that biomaterials including

cellulose contain electron-donor groups. Due to the high redox potential (above +1.3 V at standard condition), Cr(VI) can be easily reduced to Cr(III) by the biomaterials in acidic conditions.[43] Actually, even if unmodified CNFs were used for Cr(VI) adsorption, a considerable amount of Cr(III) ions could be detected in the resultant solutions (data not shown). In addition, for PAMAM-g-CNFs, the electrons for such a redox reaction might also come from the amine groups on the biosorbents.[27] Furthermore, kinetics and thermodynamics studies consistently manifested that some chemical reactions indeed happened during the adsorption process.

The Cr(VI) removal mechanism by PAMAM-g-CNFs aerogel was complicated. Both ion exchange and redox reaction were involved in this process. The proposed mechanism was depicted in Figure 4c. Initially, amine groups were protonated in acidic conditions, and the Cr(VI) ions were electrostatically attracted by PAMAM-g-CNFs. Then, part of Cr(VI) was reduced to Cr(III) by adjacent electron-donor groups. Finally, part of Cr(III) was released into the aqueous phase owing to electronic repulsion between the positively-charged groups and the Cr(III), while some Cr(III) ions could still interact with the negatively charged groups on PAMAM-g-CNFs to form a stable complex (Figure 4c).

Regeneration study

Excellent reusability is desired to reduce the amount of adsorbent materials, thereby lowering the material costs for Cr(VI) removal. The reuse potential of PAMAM-g-CNFs was evaluated and the results were shown in Figure 6a. It was observed that adsorption capacity decreased to 84.4% for the first cycle, then the decrease slowed down for the subsequent recycling. Although the removal decreased to 76.0% after the 3rd cycle, it was still as high as 255.34 mg/g, which remained to be superior to those of almost all other biosorbents even used for the first time (Table 1).

Effect of the presence of other anions

In many cases, waste water contains various kinds of anions, which can compete with the Cr(VI) ions for adsorption. In this study, the effect of different anions

including NO_3^- ($NaNO_3$), SO_4^{2-} (Na_2SO_4), and $H_2PO_4^-$ (KH_2PO_4) on Cr(VI) removal was studied and the results were shown in Figure 6b. The removal of Cr(VI) in the presence of 0.01M SO_4^{2-} was 70.5% of that for neat Cr(VI) solution, whereas it was 80.0% and 93.5% for 0.01M $H_2PO_4^-$ and NO_3^-, respectively. This could be explained by the different affinities of ions toward PAMAM-g-CNFs, which mainly depended on the ion charge density. The Z/r (charge/radius) value of SO_4^{2-} is greater than those for NO_3^- and $H_2PO_4^-$ and multivalent anions are adsorbed more readily than monovalent anions.[44] Notably, under acidic conditions, part of $H_2PO_4^-$ will be transformed into HPO_4^{2-} and PO_4^{3-}, which have greater ion charge density and affinity.[42] As a result, the decreasing trend of Cr(VI) removal in the presence of competing anions was observed in the order of: $NO_3^- < H_2PO_4^- < SO_4^{2-}$.

Conclusions

In this study, a novel dendrimer PAMAM-g-CNFs aerogel was prepared and it adsorption properties on the hazardous Cr(VI) were investigated. Due to its very high porosity, large specific surface area and abundant nitrogen-containing groups, the PAMAM-g-CNFs exhibited a fascinating adsorption performance. The maximum Cr(VI) adsorption capacity of the aerogel was 377.36 mg/g, the highest one ever reported for any biosorbents. Interestingly, it was discovered that Cr(VI) could be effectively reduced to the much less toxic Cr(III), suggesting that PAMAM-g-CNFs aerogel was capable to detoxify Cr(VI). Owing to the excellent Cr(VI) removal performance as well as the intrinsic biodegradability and environmental friendliness of cellulose, the PAMAM-g-CNFs aerogel is expected to become a promising adsorbent for scale up practice on environmental remediation.

Acknowledgements

The authors would like to thank National Natural Science Foundation of China (51303112, 51473100 and 51433006) and Young Talent Program for Science and Technology Innovation of Sichuan Provincial Government (2015089) for financial

support of this work.

Reference:

1 P. Wang and I. M. C. Lo, *Water Res.*, 2009, **43**, 3727.

2 H. Wang, X. Yuan, Y. Wu, G. Zeng, X. Chen, L. Leng, Z. Wu, L. Jiang and H. Li, *J. Hazard. Mater.*, 2015, **286**, 187.

3 J. Zhu, S. Wei, H. Gu, S. B. Rapole, Q. Wang, Z. Luo, N. Haldolaarachchige, D. P. Young and Z. Guo, *Environ. Sci. Technol.*, 2012, **46**, 977.

4 X. Sun, L. Yang, Q. Li, J. Zhao, X. Li, X. Wang and H. Liu, *Chem. Eng. J.*, 2014, **241**, 175.

5 J. Wang and C. Chen, *Biotechnol. Adv.*, 2009, **27**, 195.

6 D. Ozdes, A. Gundogdu, B. Kemer, C. Duran, M. Kucuk and M. Soylak, *Can. J. Chem. Eng.,* 2014, **92**, 139.

7 K. Kaya, E. Pehlivan, C. Schmidt and M. Bahadir, *Food Chem.,* 2014, **158**, 112.

8 F. H. Jumean, M. I. Khamis, Z. A. Sara and M. S. AbouRich, *Am. J. Anal. Chem.,* 2015, **6**, 47.

9 R. Yang, K. B. Aubrecht, H. Ma, R. Wang, R. B. Grubbs, B. S. Hsiao and B. Chu, *Polymer,* 2014, **55**, 1167.

10 R. J. Moon, A. Martini, J. Nairn, J. Simonsen and J. Youngblood, *Chem. Soc. Rev.*, 2011, **40**, 3941.

11 D. Klemm, F. Kramer, S. Moritz, T. Lindstrm, M. Ankerfors, D. Gray and A. Dorris, *Angew. Chem. Int. Ed.*, 2011, **50**, 5438.

12 Y. Xia, R. Mokaya, G. S. Walker and Y. Zhu, *Adv. Energy. Mater.*, 2011, **1**, 678.

13 A. P. Katsoulidis and M. G. Kanatzidis, *Chem. Mater.*, 2011, **23**, 1818.

14 Y. Zhou, C. Fuentes-Hernandez, T. M. Khan, J.-C. Liu, J. Hsu, J. W. Shim, A. Dindar, J. P. Youngblood, R. J. Moon and B. Kippelen, *Scientific reports*, 2013, doi:10.1038/srep01536.

15 X. Yang and E. D. Cranston, *Chem. Mater.*, 2014, **26**, 6016.

16 Q. Zhang, N. Wang, L. Zhao,T. Xu and Y. Cheng, *ACS Appl. Mater. Inter.,* 2013, **5**,

1907.

17 A.-M. Caminade and J.-P. Majoral, *Chem. Soc. Rev.*, 2010, **39**, 2034.

18 K. N. Han, B. Y. Yu and S.-Y. Kwak, *J. Membrane Sci.,* 2012, **396**, 83.

19 M. S. Diallo, K. Falconer, J. H. Johnson and W. A. Goddard, *Environ. Sci. Technol.,* 2007, **41**, 6521.

20 Y. Si, J. Yu, X. Tang, J. Ge and B. Ding, *Nat. Commun.*, 2014, doi:10.1038/ncomms6802.

21 X. Wang, L. Chen, F. Li, K. Chen, W. Wan and Y. Tang, *J. Hazard. Mater.*, 2010, **175**, 816.

22 Q. Zhang, N. Wang, T. Xu and Y. Cheng, *Acta Biomater.*, 2012, **8**, 1316.

23 B. Pan, F. Gao and H. J. Gu, *J. Colloid Interf. Sci.*, 2005, **284**, 1.

24 M. Das, S. Patil, N. Bhargava, J.-F. Kang, L. M. Riedel, S. Seal and J. J. Hickman, *Biomaterials*, 2007, **28**, 1918.

25 H.-J. Jacobasch, G. Baub6ck and J. Schurz, *colloid polym. sci.,* 1985, **263**, 3.

26 S. Deng, and Y. P. Ting, Environ. *Sci. Technol.,* 2005, **39**, 8490.

27 B. Liu and Y. Huang, *J. Mater. Chem*., 2011, **21**, 17413.

28 Y. Ku and I. Jung, *Wat. Res.*, 2001, **35**, 135.

29 W. T. Tan, S. T. Ooi and C. K. Lee, *Environ. Technol.,* 1992, **14**, 277.

30 G. Moussavi and B. Barikbin, *Chem. Eng. J.,* 2010, **162**, 893.

31 I. Langmuir, *J. Am. Chem. Soc.*, 1918, **40**, 1361.

32 C. Shuang, P. Li, A. Li, Q. Zhou, M. Zhang and Y. Zhou, *Wat. Res.*, 2012, **46**, 4417.

33 V. K. Gupta, D. Pathania, S. Agarwal and S. Sharma, *Environ. Sci. Pollut. R.*, 2013, **20**, 2632.

34 H. W. Kwak, M. K. Kim, J. Y. Lee, H. Yua, M. H. Kim, Y. H. Park and K. H. Lee, *Algal Res.,* 2015, **7**, 92.

35 P Lakshmipathiraj, S Umamaheswari, G. B. Raju, S. Prabhakar, G. Caroling, S. Kato and T. Kojima, *Environ. Prog. Sustain.*, 2013, **32**, 35.

36 L. Sun, Z. Yuan, W. Gong, L. Zhang, Z. Xu, G. Su and D. Han, *Appl. Surf. Sci.,* 2015, **328**, 606.

37 Z. Song, W. Li, W. Liu, Y. Yang, N. Wang, H. Wang and H. Gao, *RSC Adv.,* 2015, **5**, 13028.

38 J. Zhang, T. Shang , X. Jin, J. Gao and Q. Zhao, *RSC Adv.,* 2015, **5**, 784.

39 W. Song, B. Gao, T. Zhang, X. Xu, X. Huang, H. Yu and Q. Yue, *Bioresource Technol.,* 2015, doi:10.1016/j.biortech.2015.01.103.

40 Y. S. Ho, *J. Hazard. Mater.*, 2006, **136**, 681.

41 H. Demiral, I. Demiral, F. Tumsek and B. Karabacakoglu, *Chem. Eng. J.*, 2008, **144**, 188.

42 L. Dupont and E. Guillon, *Environ. Sci. Technol.*, 2003, **37**, 4235.

43 D. Park, Y. S. Yun and J. M. Park, *Environ. Sci. Technol.*, 2004*,* **38***,* 4860.

44 L. Lv, J. He, M. Wei, D.G. Evans and X. Duan, *J. Hazard. Mater.*, 2006, **133**, 119.

452 **Table 1.** Comparison of the maximum Cr(VI) adsorption capacities of various
453 biosorbents.

adsorbent	q_{max} (mg/g)	reference
Tartaric acid modified wheat bran	5.28	7
Ficus carica bast fiber	19.68	33
Spirulina platensis extract	41.12	34
Strychnos potatorum seed	59	35
Sheep wool	64.5	8
Thiol-modified cellulose nanofibrous composite membranes	87.5	9
Fe^0 nanorods modified with chitosan in porous anodic alumina	118.76	36
Magnetic lignin composite modified with diethylenetriamine	123	37
Pinus brutia	140.8	6
Nitrogen-enriched activated carbon based bamboo	142.9	38
Amine-functionalized magnetic corn stalk composites	158.73	39
Amino-functionalized magnetic cellulose nanocomposite	171.5	4
Dendrimer poly(amidoamine)-grafted cellulose nanofibril aerogels	377.36	This study

454

Figure Captions

Figure 1. Photographs of the water dispersions of (a) OCFs and (b) CNFs after three days standing. (c) The schematic for the synthesis of PAMAM-g-CNFs.

Figure 2. (a) Photograph of a piece of PAMAM-g-CNFs aerogel standing on top of lily stamen. (b) SEM images on the cross-section of aerogel. (c) FTIR spectra of CNFs and PAMAM-g-CNFs. (d) XPS N_{1s} core-level spectrum of G5.

Figure 3. (a) Effect of pH on Cr(VI) adsorption. (b) Langmuir and Freundlich isotherms for Cr(VI) adsorption. (c) Effect of nitrogen content on Cr(VI) adsorption. Photographs of the Cr(VI) solution (d) before and (e) after adsorption, and the Cr(VI) complextion with 1,5-diphenylcarbazide (f) before and (g) after adsorption.

Figure 4. (a) The Cr(VI) adsorption curve with contacting time (inset image: pseudo-second-order kinetics plot). (b) Effect of temperature on Cr(VI) removal (inset image: thermodynamic fitting curve).

Figure 5. (a) XPS Cr_{2p} spectrum for G5 after Cr(VI) adsorption. (b) Dynamics of Cr(VI) and Cr(III) concentrations in solution during the adsorption process. (c) Proposed mechanism of Cr(VI) removal by PAMAM-g-CNFs.

Figure 6. (a) Removal efficiency (%) of Cr(VI) by PAMAM-g-CNFs at different regeneration cycles. (b) Effect of competing anions on the removal efficiency (%) of Cr(VI).

475 **Figure 1.**

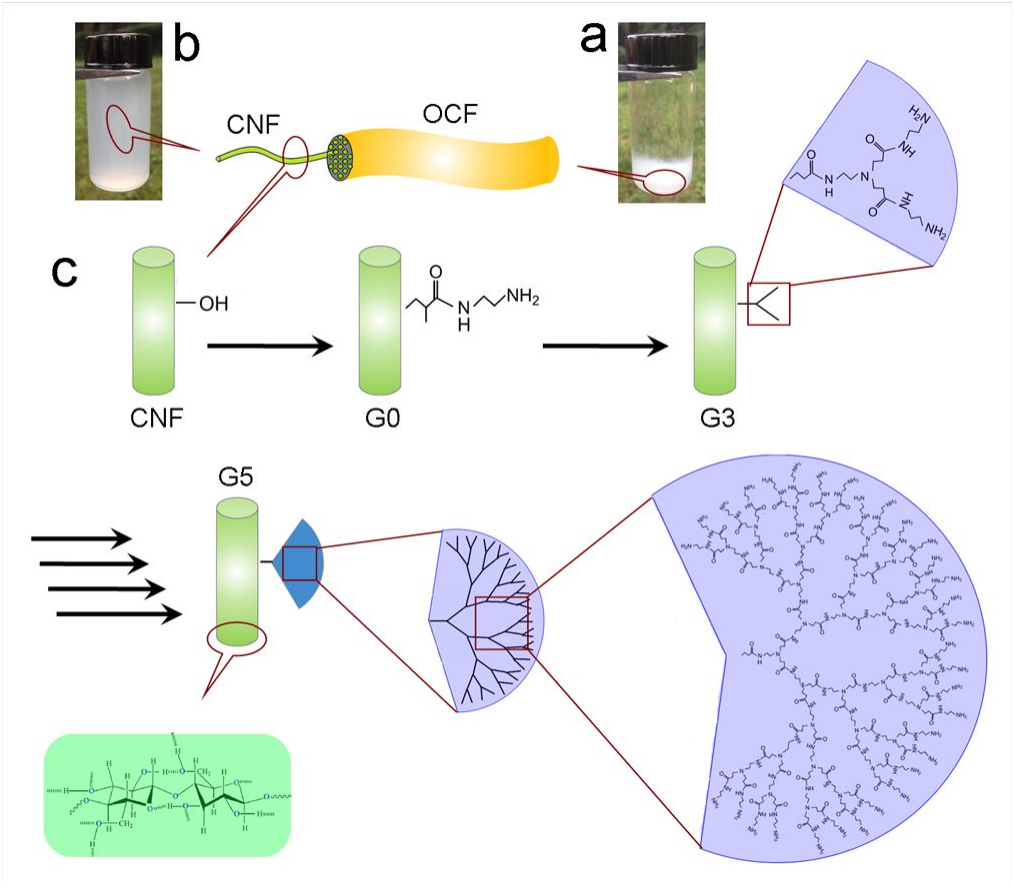

476

477

478 **Figure 2.**

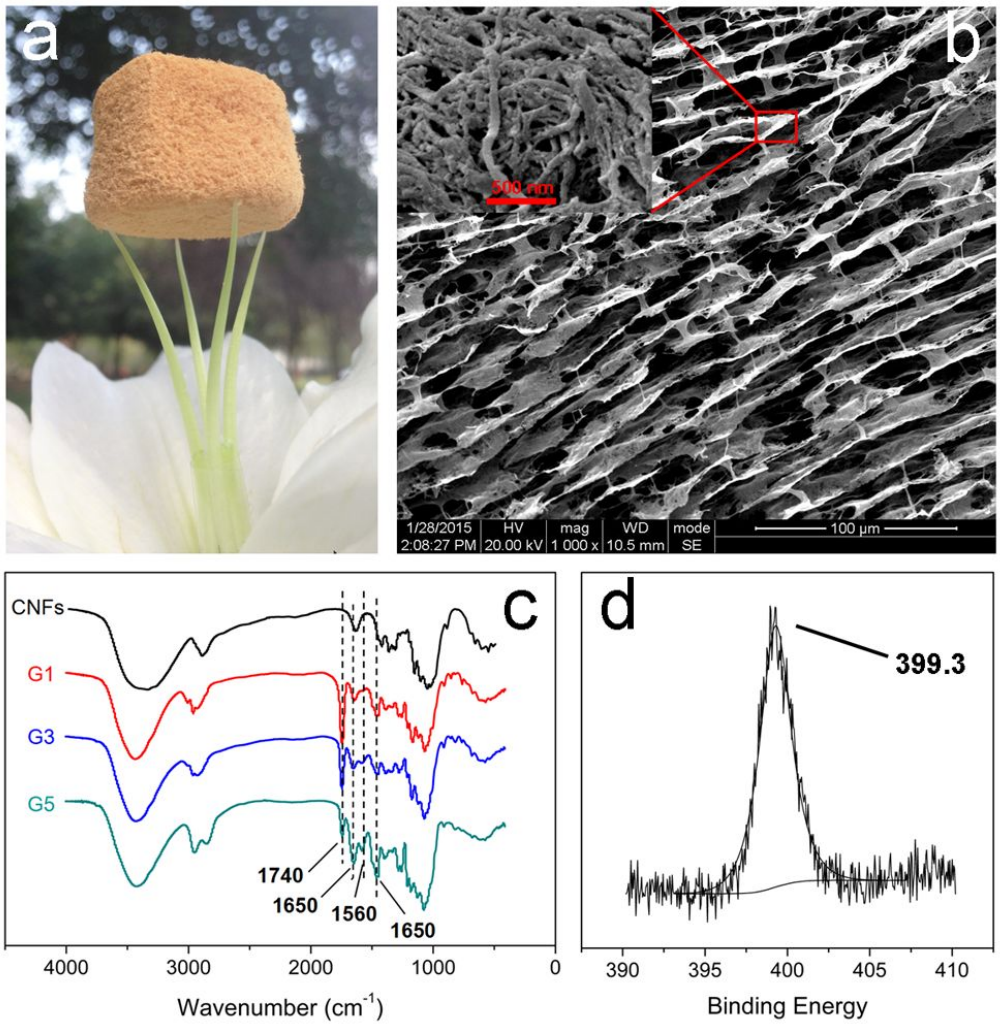

479

480

481 **Figure 3.**

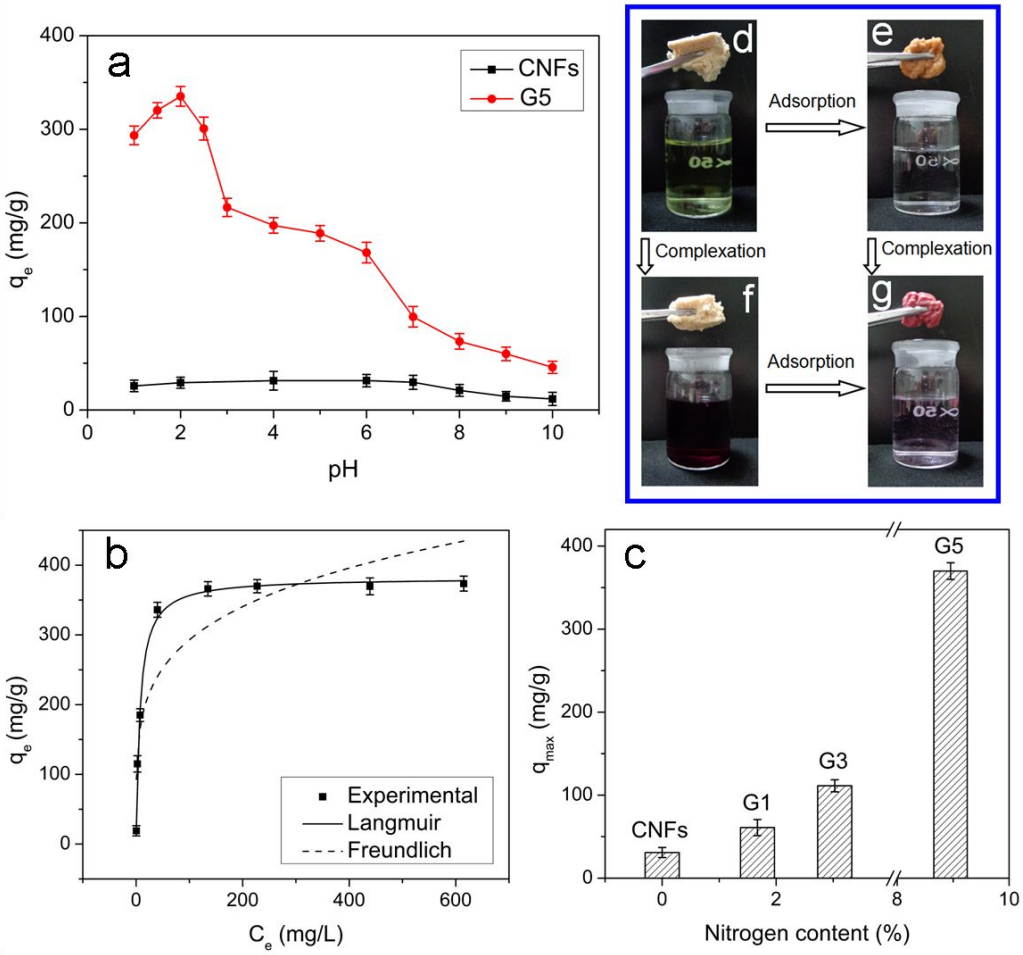

482
483

484 **Figure 4.**

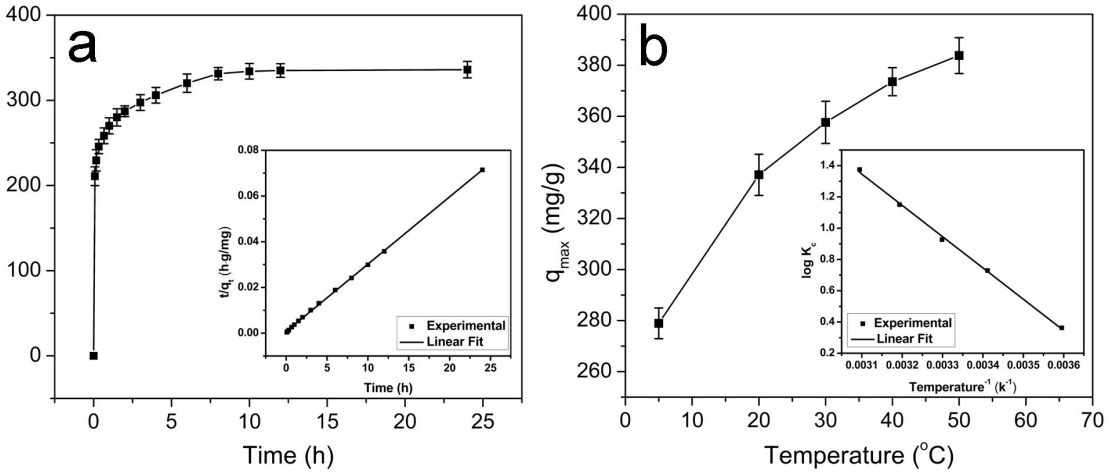

485

486

487 **Figure 5.**

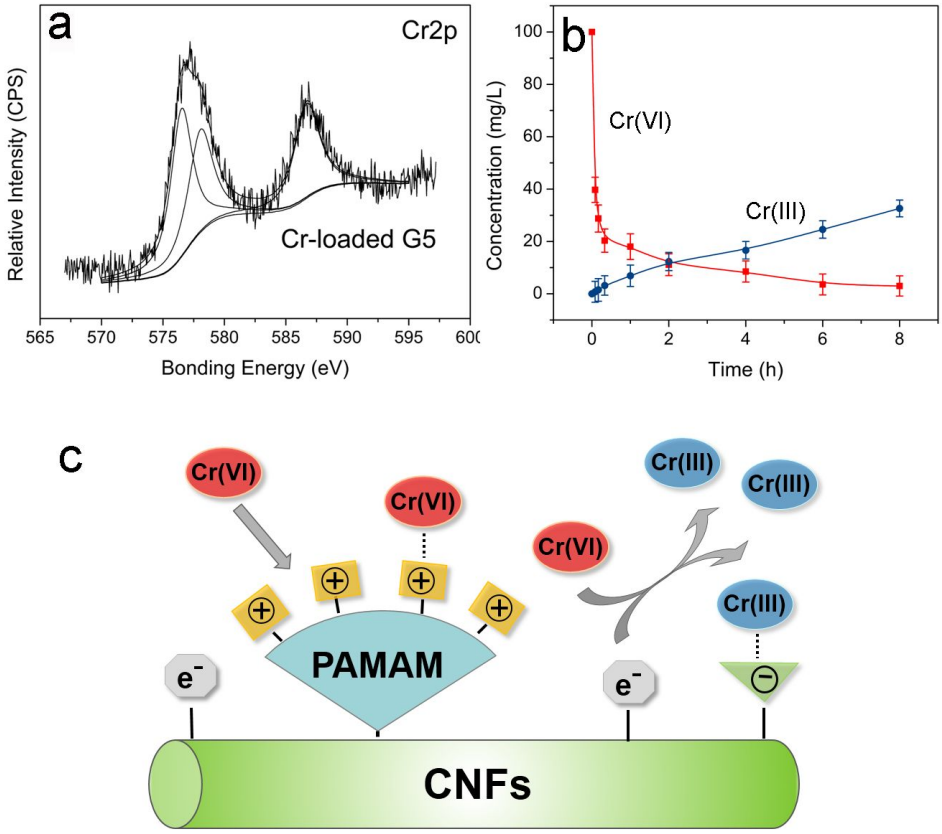

488

489

490 **Figure 6.**

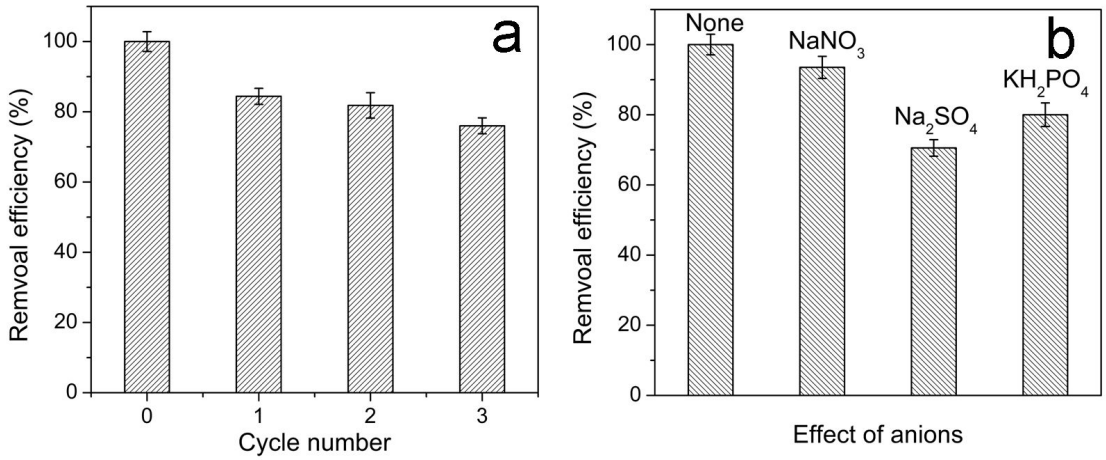

491

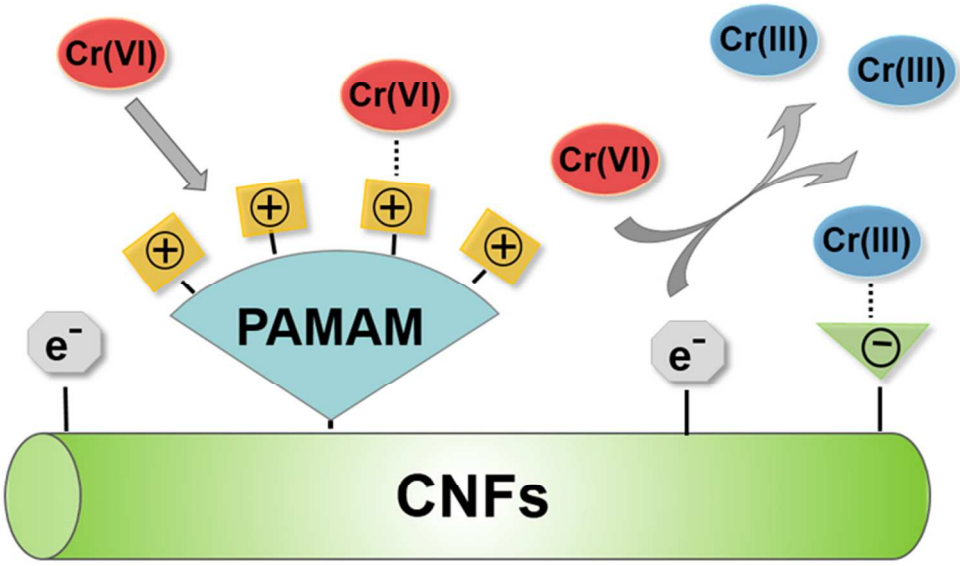

A dendrimer PAMAM-g-CNFs aerogel with unique molecular and microscropic structures demonstrates outstanding performance on Cr(VI) removal.
66x39mm (300 x 300 DPI)